Nano Energy 48 (2018) 161–169

Contents lists available at ScienceDirect

Nano Energy

journal homepage: www.elsevier.com/locate/nanoen

Full paper

Photonic surface waves enabled perfect infrared absorption by monolayer graphene

Qianru Yang[a,b], Cheng Zhang[a,b], Shaolong Wu[a,b], Shaojuan Li[c], Qiaoliang Bao[c,d], Vincenzo Giannini[e,f], Stefan A. Maier[e,g], Xiaofeng Li[a,b,*]

[a] College of Physics, Optoelectronics and Energy & Collaborative Innovation Center of Suzhou Nano Science and Technology, Soochow University, Suzhou 215006, China
[b] Key Lab of Advanced Optical Manufacturing Technologies of Jiangsu Province & Key Lab of Modern Optical Technologies of Education Ministry of China, Soochow University, Suzhou 215006, China
[c] Institute of Functional Nano and Soft Materials (FUNSOM), Jiangsu Key Laboratory for Carbon-Based Functional Materials and Devices, and Collaborative Innovation Center of Suzhou Nano Science and Technology, Soochow University, Suzhou 215123, China
[d] Department of Materials Science and Engineering, ARC Centre of Excellence in Future Low-Energy Electronics Technologies (FLEET), Monash University, Clayton, Victoria 3800, Australia
[e] Blackett Laboratory, Imperial College London, Prince Consort Road, London SW7 2BZ, United Kingdom
[f] Instituto de Estructura de la Materia (IEM-CSIC), Consejo Superior de Investigaciones Cientificas, Serrano 121, 28006 Madrid, Spain
[g] Chair in Hybrid Nanosystems, Nanoinstitute Munich, Faculty of Physics, Ludwig-Maximilians-Universität München, 80799 München, Germany

ARTICLE INFO

Keywords:
Surface wave
Bloch surface wave
Graphene perfect absorber
Thin-film optics
Admittance loci

ABSTRACT

The low absorptivity of monolayer or few-layer graphene is one of the key limitations for high performance. To improve the graphene absorption, highly nanostructured or metallic systems have been usually employed, which however rely on the advanced nanofabrication with high cost or strong metallic parasitic absorption. In this study, via thin-film optics, the photonic surface waves based on purely dielectric planar system are proposed to realize perfect optical absorption by monolayer graphene with the thickness of ~ 0.34 nm. The Bloch surface wave (BSW) is found to be excited efficiently from 7-layer dielectric system by carefully addressing the admittance matching conditions, electric/magnetic field confinement, and band structure. Coupling with the strongly localized BSW field, a monolayer graphene shows an absorption ~ 100% at the designed infrared band (1310 nm, which can be tuned readily). With detailedly addressing the excitation condition of BSW, it is found that the perfect absorber can also be realized based on the more generalized surface waves from aperiodic structure. It is believed that the thin-film and purely dielectric surface wave system provides two-dimensional devices a promising opportunity for low-cost and high-performance applications.

1. Introduction

In recent years, graphene has attracted considerable attention in photonic, optoelectronic, and related fields due to their unique physical, optoelectronic, and mechanical benefits [1–4], including atomical thickness (~ 0.34 nm) [5], crossed energy band structure allowing wavelength-independent absorption in a broad spectral range [6,7], extremely high carrier mobility (~ 2.5×10^5 cm^2 V^{-1} s^{-1} at room temperature) [3], high flexibility and conductivity [2], etc. Recent studies have also shown that intrinsic plasmons can be stimulated in graphene and readily tuned by controlling its Fermi energy [8–11]. Although graphene has witnessed versatile applications, e.g., photoconversion/photodetection [4,12–15], the low absorption of graphene, especially by monolayer or few-layer graphene, keeps to be one of the key limitations on the performance of the graphene-based optoelectronic systems. The absorptivity of a monolayer graphene under normal incidence is only 2.3% of incident light [6], defined by the fine structure constant; for intense light irradiation, the graphene layer becomes almost transparent bleached due to the filled conduction band or evacuated valence band [8].

Therefore, substantially improving the absorption of graphene is a prerequisite for its widespread applications. Strategies to enhance the graphene absorptivity are exemplified as following. i) Surface plasmon polaritons (SPPs): *combining graphene with conventional noble plasmonic nanostructures can extremely enhance the localized light-matter interactions so as to improve the device performance* [16,17]. In addition, graphene can support intrinsic plasmons which have several advantages over those from conventional noble metals, e.g., high confinement of

* Corresponding author at: College of Physics, Optoelectronics and Energy & Collaborative Innovation Center of Suzhou Nano Science and Technology, Soochow University, Suzhou 215006, China.
E-mail address: xfli@suda.edu.cn (X. Li).

https://doi.org/10.1016/j.nanoen.2018.03.048
Received 16 August 2017; Received in revised form 5 February 2018; Accepted 17 March 2018
Available online 19 March 2018

electromagnetic field, a longer lifetime of polaritons, and tunable plasmon dispersion [9–11,18-20]. The photodetector based on graphene intrinsic plasmons leads to the photocurrent enhancement by an order of magnitude [21]. ii) Waveguides: for example, CMOS-compatible graphene photodetector consists of a waveguide coated by graphene so that the light confined in the waveguide can be more effectively absorbed by graphene layer [22–25]. iii) Microcavity: the graphene layer is sandwiched by top and bottom highly reflective distributed Bragg reflectors (DBRs) so that strong light-graphene coupling can be achieved as a result of the multiple-reflection interference effect; with microcavity, literature indicates that the responsivity reaches 21 mA/W with an absorption enhancement over 60% [26].

It is noteworthy that most of these advanced light-trapping strategies for graphene are based on the highly nanostructured configurations, including plasmonics or metamaterials by the nanopatterned metallic systems or microcavity composed by tens of dielectric layers. Furthermore, the existence of metallic component often leads to a high parasitic absorption, which constrains the graphene absorption. To this regard, the recurrence of the conventional non-metal planar systems could be a promising solution since it can not only simplify the system configuration for low-cost fabrication but also offer better compatibility to the current photonic systems [2]. Moreover, for planar setups, minimizing the number of thin-film layers as well as the overall device thickness is of critical importance for developing a cost-effective photonic or optoelectronic system [26,27]. Therefore, the investigation of a few-layer planar system with strong optical absorption is urgently desired to promote the progress of graphene optoelectronics.

According to the photonic theory, Bloch surface waves (BSWs) belong to a special kind of photonic wave which can be excited from multilayered planar systems. Like SPPs, BSW system can confine the electromagnetic energy in a deep-subwavelength region very close to the surface; the difference is that the resonant wavelength of BSW can be readily manipulated by controlling the photonic bandgap and the defect layer of the photonic crystal (PC). As BSW can break the optics diffraction limit [28], it allows numerous potential applications in optoelectronic systems as an alternative mechanism of SPPs. In this report, taking the advantages of the strong field localization and purely dielectric composition of BSWs, we configure monolayer graphene onto the BSW system and propose BSW-assisted graphene perfect absorber (B-SGPA). It can substantially improve the absorption performance of the atomically thin graphene layer. We first briefly study the excitation and photonic band properties of BSW in a 7-layer dielectric system, which is followed by the incorporation of monolayer graphene. Electromagnetic calculation indicates that under the excitation of BSW, the monolayer graphene exhibits the perfectly 100% absorption assisted by the BSW coupling. The underlying physics and the photonic controllability of the BSW for achieving the perfect absorption in monolayer graphene are further discussed by analyzing the admittance loci. Especially, the admittance matching condition for perfect absorption are presented. Based on the above understanding, we propose a convenient photonic design which can rapidly realize perfect absorption in graphene. Finally, the photonic design for the perfect monolayer graphene absorber is extended to the more generalized surface wave system, i.e., an aperiodic surface wave system. It is believed that the surface wave approach to realize the perfect absorption of monolayer graphene affords a promising platform for fabricating low-cost and high performance optoelectronic devices based on two-dimensional (2D) materials.

2. BSW physics and treatments

BSW is a kind of surface electromagnetic wave which propagates along the interface between a truncated PC and a homogeneous medium. Like SPPs and Tamm plasmons [27,29], BSWs show very strong electromagnetic confinement/enhancement in the near-field region of the interface [28,30]. The inset of Fig. 1a illustrates the schematic of the multilayer (7 layers) planar system for BSW excitation, where the light blue region represents the K9 glass prism (light-injection side), the three-pair PC is composed of alternating TiO_2/MgF_2 (thickness: 225 nm/272 nm) layers, and the defect layer is a 25 nm thick TiO_2 layer. Unless specific indication, above parameters are fixed and the source has the transverse electric (TE) polarization. In fact, under transverse magnetic (TM) illumination, BSWs can also be excited, but under distinct system parameters.

Such a multilayer optical system can be simulated by using the semi-classical optical treatment, i.e., the transfer matrix method (TMM). The details on TMM of the BSW and generalized surface-wave photonic system are given in Section 1 of Supplementary information, where the admittance loci and the TMM for the monolayer graphene have also been provided (these will be discussed later in this study).

In addition, the excitation of BSWs can be simplified by the virtual cavity approximation and evaluated by using the admittance matching condition. More specifically, the virtual cavity approximation assumes the existences of two highly-reflective mirrors, which sandwich a cavity without physical thickness. On one hand, the defect-incorporated PC composes mirror I with a high reflection within the photonic gap; on the other hand, since the admittance of air is purely imaginary under an incident angle over the critical angle, i.e., total internal reflection (TIR), the air/structure interface shows a very strong reflection, namely, mirror II. Therefore, the BSWs can be excited from the cavity under the resonant conditions. More details of the virtual cavity model together with the relevant discussions can be found in Section 2 of Supplementary information.

Fig. 1a shows the photonic bandgap and dispersion relation of the considered BSW system. It reveals that BSWs just appear within the photonic gap, where the light propagation is normally prohibited. Our calculation on the BSWs is based on admittance matching in terms of the TMM (see Section 1 of Supplementary information), which will be used to further design and unveil the physics of the BSWs in the following sections. Although BSWs belong to a kind of guided mode [30], their coupling method due to photonic gap differs fundamentally from the conventional guided modes in the multilayer planar dielectric system, e.g., BSWs propagate along interface rather than within the physical cavity. Fig. 1b plots the electric and magnetic field distributions of a BSW at the wavelength of $\lambda = 1.31$ μm and an incident angle of 45°. It is obvious that the field confinement of BSWs is quite similar to that of SPPs, i.e., the electric field is peaked very near the top surface and decreases exponentially away from the interface. However, the most benefit of BSWs compared with SPPs lies in that there is no parasitic metallic absorption, allowing lossless manipulation of the light. We thus believe that the BSW system can be the very promising candidate for energy harvesting based on extremely thin absorber. A typical example of this application is the 2D materials represented by graphene, which normally shows an extremely low absorption if without using any photonic designs.

3. Result and discussion

3.1. BSW-assisted graphene perfect absorber (B-SGPA)

It is fairly straightforward to incorporate the graphene layer into the BSW system as shown in Fig. 2a, where the Kretschmann configuration (K9 glass, $n_{K9} = 1.5032$) for phase matching and TiO_2 (refractive index $n_{TiO2} = 2.3$, thickness $d_{TiO2} = 225$ nm) and MgF_2 ($n_{MgF2} = 1.38$, $d_{MgF2} = 272$ nm) act as alternating non-absorbing dielectric materials (layers 1–6). Layer 7 is the TiO_2 defect layer with $d_{defect} = 25$ nm and the top layer (8th layer) is the monolayer graphene (0.34 nm) with surface conductivity $\sigma = e^2/(4\hbar)$. The introduced graphene layer is regarded as an ideal 2D material with an atomical thickness and the corresponding TMM treatment is shown in Section 1 of Supplementary information. The reflection, transmission, and absorption spectra of B-SGPA are depicted in Fig. 2b. It should be noted that the system is designed to

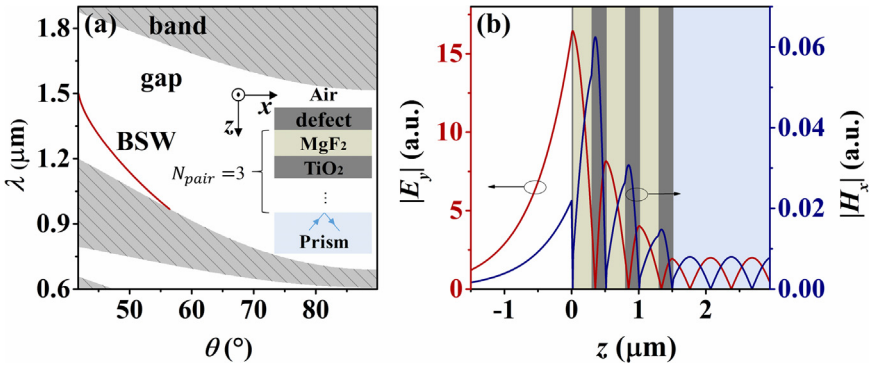

Fig. 1. (a) Dispersion curve (red line) of Bloch surface wave. Gray (white) regions represent the bands (gaps) of an ideal photonic crystal. (b) The profiles of amplitude of electric and magnetic tangential components, i.e., $|E_y|$ (red line) and $|H_x|$ (blue line), along z axis with the incident angle of 45° at the wavelength of 1.31 μm. Calculation is based on admittance matching whose details are shown in Section 2 of Supplementary information. Device configuration is inserted into (a), which is composed of three pairs PC of alternating TiO_2/MgF_2 (225 nm/272 nm) layers and 25 nm TiO_2 defect layer.

have the BSW excitation at the wavelength of 1.31 μm. Our result indicates that the excitation of BSW has indeed extremely enhanced absorption of the monolayer graphene to reach unity (A ≈ 99.99991%), showing almost zero reflection and zero transmission. This is an outstanding improvement of the optical performance of the monolayer graphene since it has just the thickness of 0.34 nm with bare absorption ~ 2.3%. As shown in Fig. 2b, the graphene absorption drops rapidly (to be < 20%) when shifting the incident wavelength away from the BSW resonance, enabling highly sensitive and narrowband photodetection by monolayer graphene. Moreover, we would like to indicate that the decaying property of the electric field inside the PC layers is critically important to ensure the perfect absorption of the graphene layer. That means the electric field has to be decayed from the peak around the surface to zero at the PC/substrate interface so that the zero reflection by the device can be realized. Here, the electric field in the substrate (prism) is not zero in Fig. 2c due to the existence of the light injection.

Plotted in Fig. 2d is the absorption versus the incident angle and wavelength, where the narrow-band absorption peak is identified to be from the BSW. In fact, we can directly predict the excitation of BSWs by using the admittance matching condition (to be shown later in the main text with more details being given in Section 2 of Supplementary information). It is obvious that the BSW band is centered exactly by the dashed line predicted by the admittance matching condition, further verifying the importance of BSW in realizing the perfect absorption by monolayer graphene.

3.2. Photonic principle of B-SGPA

One dimensional (1D) photonic crystal is a kind of multilayer optical coating which is a mature discipline [31]. Here we use thin-film optics to analyze the optical response of the proposed graphene-based absorber. In TMM calculation, the overall matrix of the multilayer system is the multiplication of all optical matrices in all layers, which can be computed from the top to the bottom layer in sequence (or contrarily). In the matrix multiplication process, an equivalent admittance is built up from the starting layer to gradually cover all layers. Such a building-up process can be well characterized by the admittance loci. Admittance evaluation is an essential approach which is an accurate calculation derived from TMM; the great value of this method is the visualization of the phase retardation layer by layer (or even point by point). For a TMM calculation from air to the substrate, the equivalent admittance of the whole B-SGPA (excluding the substrate) is denoted as Y_{end} and the admittance of the substrate is η_s (which is a real number). It is clear that the perfect absorption should be accompanied with the zero optical reflection and transmission. Zero reflection means, i.e., the admittance matching between the multilayer system with the substrate ($Y_{end} = \eta_s$).

For the perfect optical absorption by the monolayer graphene achieved in Fig. 2b, Figs. 3a and 3c draw the admittance loci of the system by forward and backward TMM iterations, with the corresponding spatially dependent admittances being defined as $Y(z)$ and $Y'(z)$, respectively. Fig. 3a shows the admittance loci of 7 dielectric

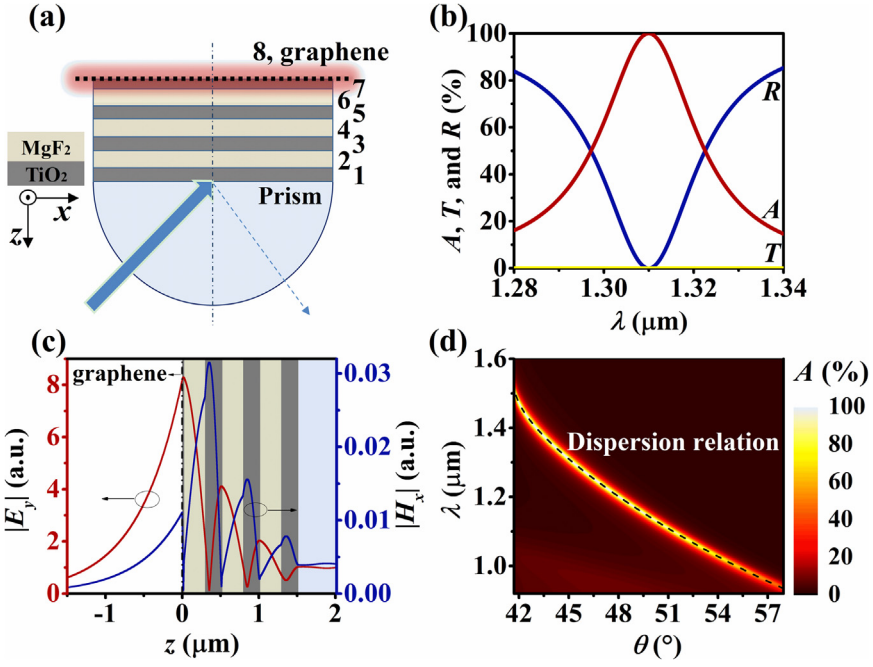

Fig. 2. (a) Schematic of BSW-assisted graphene perfect absorber (B-SGPA) whose reflection, transmission and absorption spectra under BSW are plotted in (b) with an incident angle of 45°. (c) The profiles of electric and magnetic tangential components, i.e., $|E_y|$ (red line) and $|H_x|$ (blue line), along z axis. (d) Dependences of the device absorption on incident angle and wavelength, where the dot line is the analytically calculated dispersion relation predicted according to the admittance matching condition.

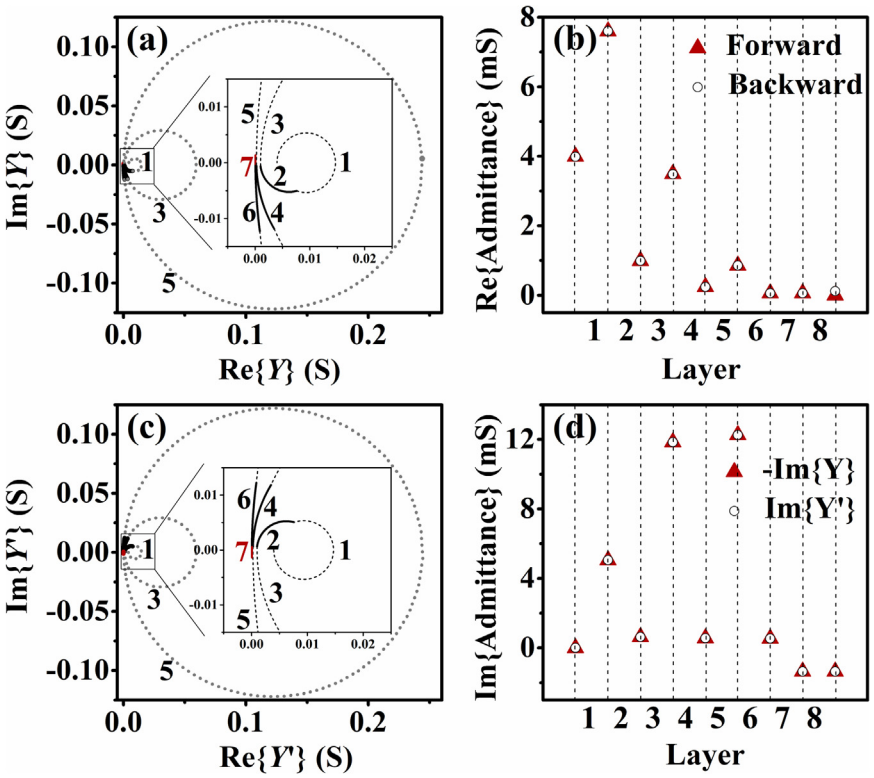

Fig. 3. Admittance loci by forward (a) and backward (c) TMM calculations, where the inserts are the enlarged views and the corresponding layer numbers are marked accordingly (see Fig. 2a). These loci are traced in anticlockwise direction. The graphene layer is undistinguishable since the variation of admittance by graphene layer is extremely tiny (see *the admittance loci of graphene layer* in Fig. S5a in Supplementary information). Red solid, black solid, and gray dot lines correspond to the defect, PC MgF_2, and PC TiO_2 layers, respectively. Real (b) and imaginary (d) parts of the admittances at interfaces between layers extracted from admittance loci.

layers (the extremely thin graphene layer is not shown). The starting point for forward TMM (air to substrate) is the free space admittance η_0 which is a purely imaginary value under an incident angle over the critical angle; the trajectory of $Y(z)$ depicted in sequence in complex plane is the admittance loci with the TMM calculation from the first interface of the device to the entire system [31]. The admittance loci are totally controlled by the thickness and optical constant of each layer under the given incident wavelength and angle. That means the destination of $Y(z)$, i.e., Y_{end}, can be controlled to match η_s through the photonic design. We have verified through Fig. 3a that $Y_{end} = \eta_s$ has been indeed realized as prediction.

In addition, we depict backward (substrate to air) admittance loci $Y'(z)$ (Fig. 3c) for backward admittance matching evaluation (graphene layer is not shown). In this case, the destination of the admittance loci is Y'_{end}. According to the calculations shown in Section 2 of Supplementary information and the numerical verification by Fig. 3c, the admittance matching condition for BSW excitation under backward TMM calculation can be written as [32–34]:

$$\mathrm{Im}\{Y'_{end} + \eta_0\} = 0 \tag{1}$$

Achieving these admittance matching conditions can ensure the excitation of BSW and graphene perfect absorption. In addition, comparing the forward and backward admittance loci (for direct observation, Fig. S5 depicts forward and backward admittance loci in each layer), we found that Y and Y' have very similar trajectories in each layer (except in graphene layer). A further insight into the admittance loci shown in Figs. 3a and 3c indicates that Y and Y' are actually mutually conjugated. This can be verified by Figs. 3b and 3d, which display the real and imaginary parts of the optical admittance in each interface between two layers. Physically, above conjugation condition is necessary for reaching perfect absorption. This is because 1) the ending point of forward admittance loci Y_{end} which matches with η_s is also the starting point of backward admittance loci in order to achieve the perfect absorption and 2) the transfer matrix of the same layer is identical, resulting in that the admittance loci follow the same circle. Since the calculations are along the contrary directions, the corresponding admittances must be conjugated. This allows to present a unified and more generalized admittance requirement for the perfect absorption: the forward and backward admittances are mutually conjugated at any position in non-absorbing media. Combining this condition with the admittance matching conditions, the requirement of B-SGPA is:

$$\begin{cases} Im\{Y'_{end} + \eta_0\} = 0 \\ Y_{end} = \eta_s \end{cases} \tag{2}$$

or

$$Y'(z) = \mathrm{conj}\{Y(z)\}, z \neq 0 \tag{3}$$

Due to the special form of graphene transfer matrix, the introduced absorbing media just breaks the admittance matching of the real part, instead of the imaginary part. Therefore, at $z = 0$, the sign of imaginary part of forward and backward admittances is opposite but with an identical absolute value. Details should refer to Section 3 of Supplementary information.

However, reaching conditions (2) or (3) is still a time-consuming process. Differing from SPPs which rely on two permittivities with opposite signs, BSW can be controlled through the modulation of electromagnetic field by multilayer system. Therefore, a convenient design can be implemented through adjusting one or several specific device parameters to reach the admittance matching for the excitation of BSW and perfect absorption. We now examine the tunability of the BSWs in the proposed B-SGPA. Fig. 4 shows the dependences of absorption spectrum on the PC pair number N_{pair}, the defect layer thickness d_{defect}, TiO_2 layer thickness in PC d_{TiO2}, MgF_2 layer thickness d_{MgF2}, and graphene Fermi energy E_F. Moreover, the schematic of barrier model is given in Fig. 4f.

Fig. 4a exhibits a high absorption region (i.e., the excitation of BSW) located in the photonic forbidden band. Although without shifting the resonant position as well as the band structure noticeably, the PC pair number N_{pair} has a strong impact on the absorptivity of the device. Specifically, when N_{pair} is too few, most of light is reflected back due to the TIR; on the contrary, with a large N_{pair}, the light is reflected directly

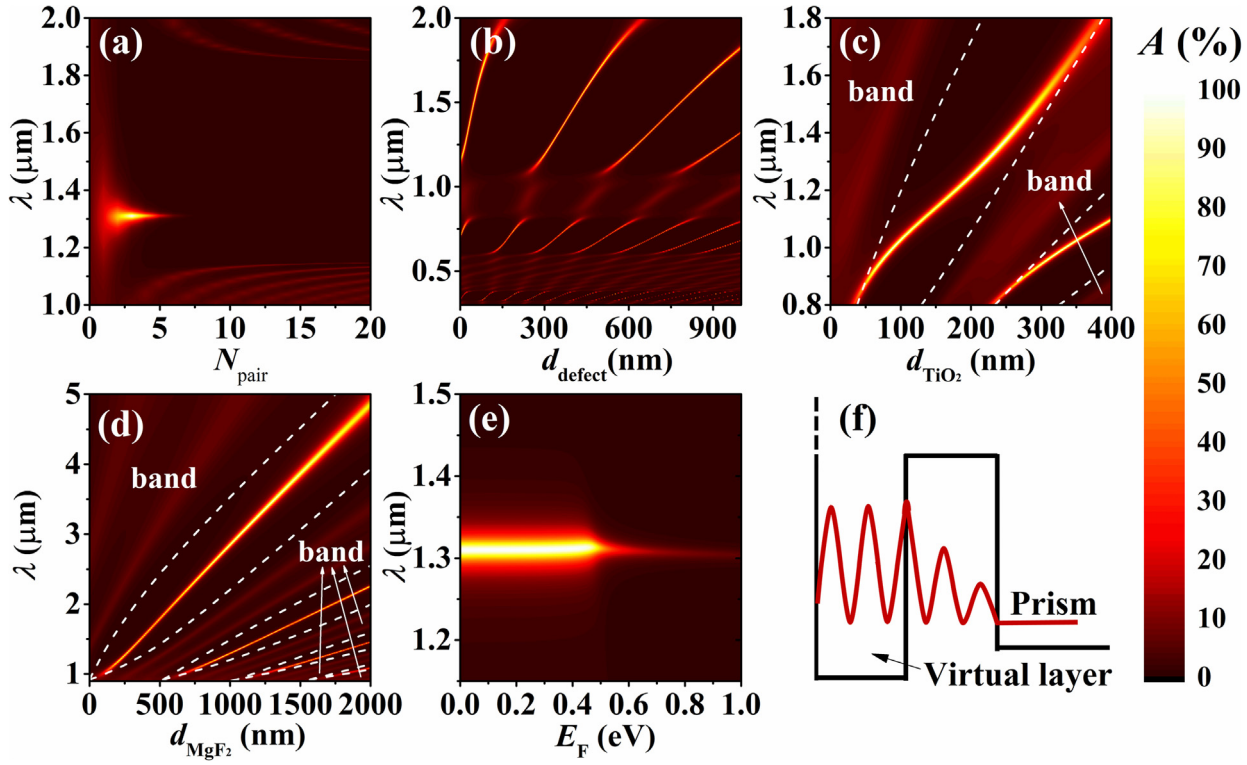

Fig. 4. Dependences of the device absorption $A(\lambda)$ on (a) d_{defect}, (b) the PC pair number N_{pair}, (c) the thickness of TiO_2 layer d_{TiO2}, (d) the thickness of MgF_2 layer d_{MgF2}, and (e) the Fermi energy of graphene E_F. The white dash lines in (c) and (d) represent the edges of photonic bandgaps. (f) The schematic of the barrier model. The rest of the parameters are the same as those indicated in the manuscript.

by PC without entering the system [27]. Further investigation indicates that increasing N_{pair} greatly alters the field attenuation and the admittance matching conditions. This can also be verified by the admittance loci shown in Fig. 3a, where the equivalent admittance gradually approaches the substrate admittance η_s with TMM calculation layer by layer. However, for a given system, if the layer number is too less, the PC effect is too weak for the whole system to reach an admittance matching with η_s; on the contrary, an over-length PC leads to the over-change of the admittance loci and consequently the mismatched admittance.

Fig. 4b shows that the defect layer affects the system absorption with a Fabry-Perot-like way; however, we may not identify it as the Fabry-Perot effect, because BSW resonates at surface, not in the defect layer. From the admittance viewpoint, the defect layer is used to control the trajectory of the admittance locus (without altering the photonic band structure of the whole system), which under some situation can show the destined admittance perfectly matched with the air (i.e., BSW excitation) repeatedly (*please see* Figs. S3 and S4). Moreover, Fig. 4b clearly shows the high/low absorption bands, corresponding to the photonic gap/band, and BSW wavelength is clearly modulated by d_{defect} which corresponds to a purely imaginary value of Bloch wavenumber that also represents the attenuation of electromagnetic field from photonic forbidden band. In B-SGPA, d_{defect} = 25 nm is an appropriate value for perfect absorption, and a larger or smaller d_{defect} may change the attenuation so that the reflected electromagnetic wave may not perfectly vanish.

A further insight into the physics behind the system can be given by a barrier model plotted in Fig. 4f, where the barrier height on the left is infinite under TIR. Here, we construct a virtual layer to illustrate the BSW resonance as suggested in literature [32]. The barrier sandwiched by the virtual layer and prism is actually composed by the graphene layer and the PC stack. Within the bandgap, the barrier hinders the light transmission; however, due to the excitation of BSW, the light under the resonant wavelength can be tunneled. The well of the virtual layer is deeper than the prism (because BSW is located within the light cone of the prism) so that the electromagnetic wave could be leaked out. The field confined by the device surface is decayed gradually and reaches zero at the barrier/prism (i.e., PC/prism) interface for perfect absorption as mentioned previously. The most effective part of this model is to view the photonic gap as a barrier with finite height and width, which is modulated by the system configurations directly. As an example, increasing d_{defect} to 40 nm leads to a higher barrier, while an increased N_{pair} can be directly considered as a wider barrier. An appropriate combination with the height and width of barrier is crucial. It is confirmed at N_{pair} = 5 (not shown), the high absorption region moves to the edge of photonic gap whose Bloch wavenumber is smaller (actually corresponding to a lower and wider barrier). Compared to controlling the defect layer, modulating the thickness of each PC layer (d_{MgF2} and d_{TiO2}) is much more effective in manipulating the BSW response since it directly alters the geometry of barrier and hence the PC properties or the band structure. Figs. 4c and 4d shows that: 1) the BSW wavelength monotonically increases with d_{MgF2} and d_{TiO2}, accompanied with the variation of the band structure; 2) the adjacent two high absorption bands are separated by the phase distance of π; 3) the low absorption band results from the guided modes in photonic band (the white dash lines represent the edges of photonic bandgaps). *In addition, it should be noticed that the BSW resonance is highly tunable to a very long-wavelength band as shown in Fig. 4d, allowing the graphene perfect absorption to occur accordingly.*

As graphene Fermi energy can be modulated easily through doping or applying gate voltage, here we briefly analyze the influence of E_F on the absorption performance of the proposed B-SGPA. Fig. 4e shows the absorption spectrum versus the Fermi energy of graphene at 300 K (graphene surface conductivity formula and other parameters are illustrated in Section 1 of Supplementary information). It is obvious that E_F does not modify the resonant wavelength. However, the absorption performance strongly depends on the comparison between E_F and ω_{BSW} ($\omega_{BSW} = 2\pi c/\lambda_{BSW}$). When $E_F < \omega_{BSW}/2$, interband process dominates

the optical response and hence B-SGPA keeps a high absorption; when $E_F > \omega_{BSW}/2$, disorder-induced trapping overwhelms the interband transition, leading to the rapidly dropped absorption [8].

Based on the above analytical and numerical studies, we would like to present a design method that can rapidly optimize the B-SGPA configuration for perfect absorption. Eq. (3) has indeed indicated that the requirements for perfect absorption are: 1) the real parts of forward and backward admittances must be equal and 2) their imaginary parts must be conjugated. The task of perfect absorption design is to control the B-SGPA configurations to achieve Eq. (3). Therefore, the controllable parameters can be numerous. The simplest way is to choose two variables; however, under which Eq. (3) might have the unique solution or no solution, i.e., it cannot ensure obtaining the optimal design of B-SGPA. Therefore, we choose three variables (d_{defect}, d_{MgF2}, and d_{TiO2}) with fixing the material refractive index, incident wavelength, and incident angle. This is because d_{defect} can adjust the resonant wavelength; at the meantime, d_{MgF2} and d_{TiO2} can finely modify the Bloch wavenumber and modulate the decaying property of the electric field inside the PC so that the admittance matching can be achieved more easily. Moreover, we find from our investigation that, although Eq. (3) has to be fulfilled everywhere inside the device, it is universally satisfied as long as this equation is confirmed at one interface. In the following design, the interface between the defect and the PC (i.e., $z = d_{defect}$) is considered, i.e., the perfect absorption condition is now simplified to $Y'(z = d_{defect}) = \text{conj}\{Y(z = d_{defect})\}$.

The above condition is evaluated by using the graphical method, i.e., plotting the conjugate forward admittances $\text{conj}\{Y(z = d_{defect})\}$ with varying d_{defect} from 0 to 322 nm and the backward admittances $Y'(z = d_{defect})$ with varying d_{MgF2} (from 0 to 745 nm) and d_{TiO2} (from 0 to 322 nm). The variation ranges considered here are selected to ensure the phase variation of π since the admittance locus will be repeated every π shift. Therefore, the overlapped region of $\text{conj}\{Y(z = d_{defect})\}$ and $Y'(z = d_{defect})$ denote the solutions of B-SGPA configuration. In fact, as shown as Fig. 5, the number of such solutions is infinite, i.e., we can find a number of possible system configurations for the BSW-graphene system to achieve perfect absorption. *Based on this method, the perfect absorption of low-loss dielectric and metal can be readily realized. For example, we have realized the perfect absorption of BSW system coated with graphene or ultra-thin metal film, with the consideration of high-performance optical sensing application* [35].

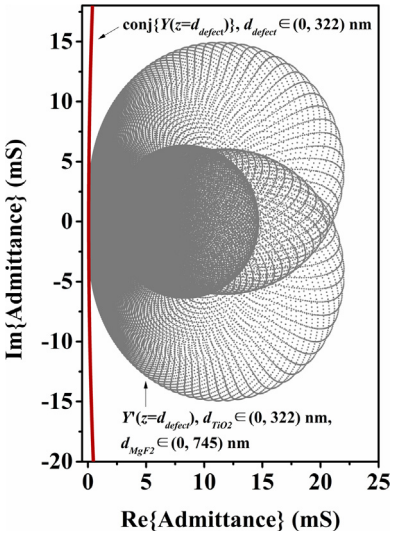

Fig. 5. Admittance matching design of B-SGPA by controlling the thicknesses of defect and PC layers. Red line is a part of the complete admittance circle by varying d_{defect}, i.e. $\text{conj}\{Y(z = d_{defect})\}$. Gray dots represent the $Y'(z = d_{defect})$ with varying d_{TiO2} and d_{MgF2}.

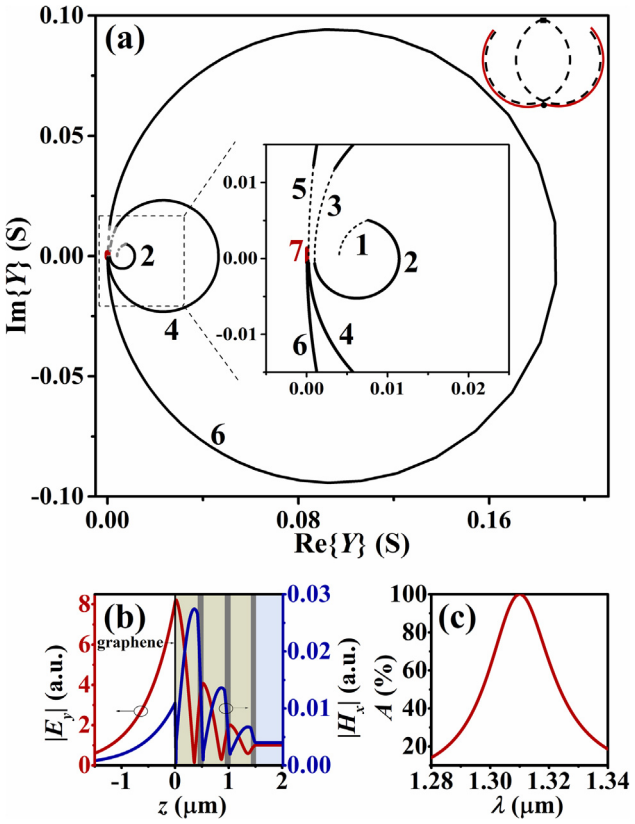

Fig. 6. (a) Admittance loci of SGPA. The example of transforming B-SGPA to SGPA is shown in the inset on top-right corner which exhibits the admittance loci of dual-layer antireflection coating system, the red solid and black dash lines represent two possible solutions for admittance evolution. (b) The profile of amplitude of electric and magnetic tangential component, i.e. $|E_y|$ (red line) and $|H_x|$ (blue line), along z axis. (c) Absorption spectrum of SGPA with the incident angle of 45°.

3.3. Surface-wave-assisted graphene perfect absorber (SGPA)

In fact, the starting and ending points of the admittance loci play the key role in determining the admittance matching, which means that there exist more than one trajectories to bridge the two terminals, i.e., allowing various photonic designs for graphene perfect absorption. For example, the inset of Fig. 6a (top-right corner) shows the case of a dual-layer antireflection coating (ARC) system [31], where the red and dashed lines indicate the two possible solutions without affecting the starting and ending admittances. From this point of view, the Bloch surface wave is not a strict requirement for perfect graphene absorber, but more generalized surface waves from aperiodic systems are also feasible, i.e., SGPA. This can be verified as follows. In fact, the example on the dual-layer ARC system reveals that the admittances on the interface between the two layers are conjugated mutually under the two designs (see the points marked by ■ and •). This allows an alternative design for the original PC in B-SGPA, i.e., to re-design the thicknesses of the TiO_2 and MgF_2 layers to ensure 1) the starting and ending points in every original PC period are unchanged and 2) the admittance in the middle interface in every original PC has a conjugated value compared to the original one. It is well known that multilayer system can improve reflection; therefore, the transformation from B-SGPA to SGPA reveals that the key requirement of surface wave assisted graphene absorption enhancement device is not photonic crystal but photonic gap or high reflection mirror. In next work, we will consider SGPA with fewer layers.

An exemplified system configuration is shown in Table 1, with the corresponding admittance loci being plotted in Fig. 6a. Compared to the admittance loci of Fig. 3a (B-SGPA), it is obvious that the admittances

Table 1
SGPA configuration.

Layer	1	2	3	4	5	6	7
Thickness (nm)	96	374.3	113.3	391.6	111.2	396.2	25

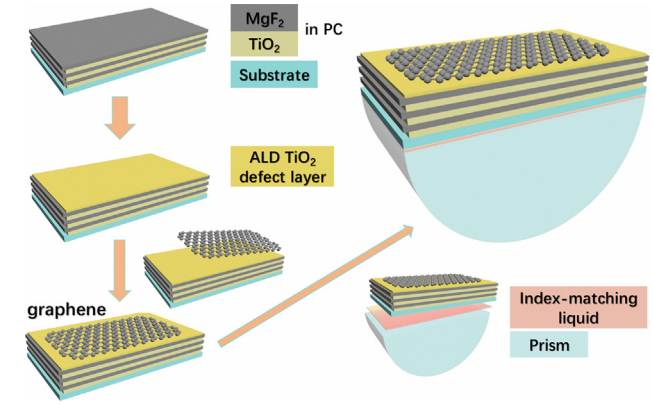

Fig. 7. Suggested fabrication procedure of the proposed B-SGPA.

on the interfaces between layers 6 and 5, 4 and 3, 2 and 1 are indeed conjugated after the new surface-wave design. Since the layer thicknesses listed in Table 1 are aperiodic (unlike the B-SGPA), the detailed trajectory of the admittance loci is distinguished from that of the B-SGPA. However, the admittances in the key interfaces are kept unchanged, ensuring the high optical absorption. Another difference lies in that the magnetic peak is shifted from TiO_2 layer (B-SGPA) toward MgF_2 layer (SGPA), see Fig. 6b. A further examination on the photonic response verifies that the absorption of the monolayer graphene can also reach 100% under the excitation of surface wave from the SGPA, see Fig. 6c.

3.4. Fabrication and measurement suggestion

A suggested fabrication procedure of B-SGPA is shown in Fig. 7. First, 3 pairs of TiO_2/MgF_2 (thickness: 225 nm/272 nm) layers are deposited in sequence by optical coating system (e.g., ion assisted deposition, IAD) on a quartz substrate. Then, a TiO_2 defect layer with thickness d_{defect} = 25 nm can be deposited on the MgF_2 layer by atomic layer deposition (ALD). Although the material of defect layer is same with that in PC, considering the significant influence of d_{defect} on resonant wavelength and the absorption of graphene (see Fig. 4b), we recommend using ALD to grow the defect layer. If different materials were chosen to construct PC or defect layer, the design approach in Fig. 5 can be used. Next, the as-prepared graphene is transferred on the ALD-grown TiO_2 defect layer (more details about graphene transfer can be found in [36]). Finally, the prism is attached to the quartz substrate by an index-matching liquid.

The measurement setup for the far-field characterization can refer to Herzig's work [37,38]. In the detection process, a rotational modulator and a tunable light source should be used to find the resonant angle and wavelength. An incident beam from NIR laser is separated as object and reference beam, where reference beam is directly sent to the detector and the object beam successively passes through collimator, diaphragm, polarizer, and diaphragm. Then, the TE-polarized light is focused and illuminated on the sample through coupling prism. Finally, after passing collection lens, the object light is detected by photodiode and sent to data acquisition (DAQ) system.

Because the vacuum light line lies above that of the prism, light cannot pass through the sample, i.e., T = 0. The detected reflection can derive the absorption of system. To verify the absorption enhancement of graphene, the BSW system without graphene has to be measured in advance to exclude the losses from other components, such as prism reflection and dielectric absorption loss.

4. Conclusions

In conclusion, we reported that the photonic design enables a promising opportunity for monolayer graphene to achieve perfect absorption at infrared band (1310 nm) by purely dielectric planar configuration. Such a substantial optical performance enhancement was realized by introducing the surface waves which confine the light energy locally to strongly couple with the monolayer graphene. The design was presented gradually from photonic basics of surface waves, transfer matrix treatment, admittance loci manipulation, device absorption performance, to the extended device design. Admittance matching/loci and the virtual cavity and potential barrier models were used to reveal the physics and excitation of BSWs. The BSW system shows a high tunability on the resonance by controllably structuring the device. Moreover, a photonic design was introduced by re-routing the admittance trajectory with adjusting the device parameters so that the admittance matching can be achieved more flexibly, which allows to employ the general surface waves excited from aperiodic systems to realize the perfect absorption. This study provides a promising solution to achieve the unprecedentedly high optical performance by using the simple film systems, rather than the metallic or strongly nanostructured systems. *The observed narrow-band and high optical absorption can also find the applications of efficient optical/optoelectronic switching and high-performance sensing.* Moreover, it is helpful for lowering the fabrication cost, enabling a better compatibility with the current optoelectronic systems.

Appendix A. Supplementary information

Supplementary data associated with this article can be found in Supplementary Information_SGPA.pdf which includes: calculation method of forward and backward admittance loci/matching; *the understanding of BSW excitation with admittance matching and virtual layer model; the separated* admittance loci mentioned in main text.

Acknowledgements

We acknowledge the support from the National Natural Science Foundation of China (Nos. 61675142, 61504088, 51290273, and 91433107), the Youth 973 Program (2015CB932700), the National Key Research & Development Program (No. 2016YFA0201902), ARC (CE170100039 and FT150100450), and Priority Academic Program Development (PAPD) of Jiangsu Higher Education Institutions. Q. Bao acknowledges the support from the Australian Research Council (ARC) Centre of Excellence in Future Low-Energy Electronics Technologies (FLEET).

Competing financial interest

The authors declare no competing financial interest.

Appendix A. Supplementary material

Supplementary data associated with this article can be found in the online version at http://dx.doi.org/10.1016/j.nanoen.2018.03.048.

References

[1] F.H.L. Koppens, T. Mueller, P. Avouris, A.C. Ferrari, M.S. Vitiello, M. Polini, Nat. Nanotechnol. 9 (2014) 780–793.
[2] A.C. Ferrari, F. Bonaccorso, V. Fal'ko, et al., Nanoscale 7 (2015) 4598–4810.
[3] K.S. Novoselov, V.I. Fal, L. Colombo, P.R. Gellert, M.G. Schwab, K. Kim, Nature 490 (2012) 192–200.
[4] T. Mueller, F. Xia, P. Avouris, Nat. Photon. 4 (2010) 297–301.

[5] J.W. Weber, V.E. Calado, M.C.M. van de Sanden, Appl. Phys. Lett. 97 (2010) 091904.
[6] R.R. Nair, P. Blake, A.N. Grigorenko, K.S. Novoselov, T.J. Booth, T. Stauber, N.M.R. Peres, A.K. Geim, Science 320 (2008) (1308–1308).
[7] J.M. Dawlaty, S. Shivaraman, J. Strait, P. George, M. Chandrashekhar, F. Rana, M.G. Spencer, D. Veksler, Y. Chen, Appl. Phys. Lett. 93 (2008) 131905.
[8] T. Low, P. Avouris, ACS Nano 8 (2014) 1086–1101.
[9] A.N. Grigorenko, M. Polini, K.S. Novoselov, Nat. Photon. 6 (2012) 749–758.
[10] F.J. García de Abajo, ACS Photon. 1 (2014) 135–152.
[11] M. Jablan, H. Buljan, M. Soljačić, Phys. Rev. B 80 (2009) 245435.
[12] M.C. Lemme, F.H. Koppens, A.L. Falk, M.S. Rudner, H. Park, L.S. Levitov, C.M. Marcus, Nano Lett. 11 (2011) 4134–4137.
[13] X. Xu, N.M. Gabor, J.S. Alden, A.M. van der Zande, P.L. McEuen, Nano Lett. 10 (2010) 562–566.
[14] N.M. Gabor, J.C.W. Song, Q. Ma, N.L. Nair, T. Taychatanapat, K. Watanabe, T. Taniguchi, L.S. Levitov, P. Jarillo-Herrero, Science 334 (2011) 648–652.
[15] C.-H. Liu, Y.-C. Chang, T.B. Norris, Z. Zhong, Nanotechnology 9 (2014) 273–278.
[16] T.J. Echtermeyer, L. Britnell, P.K. Jasnos, A. Lombardo, R.V. Gorbachev, A.N. Grigorenko, A.K. Geim, A.C. Ferrari, K.S. Novoselov, Nat. Commun. 2 (2011) 458.
[17] Z. Fang, Z. Liu, Y. Wang, P.M. Ajayan, P. Nordlander, N.J. Halas, Nano Lett. 12 (2012) 3808–3813.
[18] J. Zhang, Z. Zhu, W. Liu, X. Yuan, S. Qin, Nanoscale 7 (2015) 13530–13536.
[19] Z. Fei, A.S. Rodin, G.O. Andreev, W. Bao, A.S. McLeod, M. Wagner, L.M. Zhang, Z. Zhao, M. Thiemens, G. Dominguez, M.M. Fogler, A.H. Castro Neto, C.N. Lau, F. Keilmann, D.N. Basov, Nature 487 (2012) 82–85.
[20] K. Li, J.M. Fitzgerald, X. Xiao, J.D. Caldwell, C. Zhang, S.A. Maier, X. Li, V. Giannini, ACS Omega 2 (2017) 3640–3646.
[21] M. Freitag, T. Low, W. Zhu, H. Yan, F. Xia, P. Avouris, Nat. Commun. 4 (2013) 1591.
[22] A. Pospischil, M. Humer, M.M. Furchi, D. Bachmann, R. Guider, T. Fromherz, T. Mueller, Nat. Photon. 7 (2013) 892–896.
[23] X. Gan, R.-J. Shiue, Nat. Photon. 7 (2013) 883–887.
[24] X. Wang, Z. Cheng, K. Xu, H.K. Tsang, J.-B. Xu, Nat. Photon. 7 (2013) 888–891.
[25] M. Liu, X. Yin, E. Ulin-Avila, B. Geng, T. Zentgraf, L. Ju, F. Wang, X. Zhang, Nature 474 (2011) 64–67.
[26] M. Furchi, A. Urich, A. Pospischil, G. Lilley, K. Unterrainer, H. Detz, P. Klang, A.M. Andrews, W. Schrenk, G. Strasser, T. Mueller, Nano Lett. 12 (2012) 2773–2777.
[27] C. Zhang, K. Wu, V. Giannini, X. Li, ACS Nano 11 (2017) 1719–1727.
[28] L. Yu, E. Barakat, T. Sfez, L. Hvozdara, J.D. Francesco, H.P. Herzig, Light: Sci. Appl. 3 (2014) e124.
[29] H. Da, Q. Bao, R. Sanaei, J. Teng, K.P. Loh, F.J. Garcia-Vidal, C.W. Qiu, Phys. Rev. B 88 (2013) 205405.
[30] P. Yeh, A. Yariv, C.-S. Hong, J. Opt. Soc. Am. 64 (1977) 423–438.
[31] H.A. Macleod, Thin Film Optical Filters, 4th ed, CRC Press, Boca Raton, 2010.
[32] M. Kaliteevski, I. Iorsh, S. Brand, R.A. Abram, J.M. Chamberlain, A.V. Kavokin, I.A. Shelykh, Phys. Rev. B 76 (2007) 165415.
[33] M. Xiao, Z.Q. Zhang, C.T. Chan, Phys. Rev. X 4 (2014) 021017.
[34] A.P. Vinogradov, A.V. Dorofeenko, A.M. Merzlikin, A.A. Lisyansky, Phys.-Uspekhi 53 (2010) 243–256.
[35] Q. Yang, L. Qin, G. Cao, C. Zhang, X. Li, Opt. Lett. 43 (2018) 639–642.
[36] X. Li, Y. Zhu, W. Cai, M. Borysiak, B. Han, D. Chen, R.D. Piner, L. Colombo, R.S. Ruoff, Nano Lett. 9 (2009) 4359–4363.
[37] E. Descrovi, T. Sfez, L. Dominici, W. Nakagawa, F. Michelotti, F. Giorgis, H.P. Herzig, Opt. Express 16 (2008) 5453–5464.
[38] R. Dubey, E. Barakat, M. Häyrinen, M. Roussey, S.K. Honkanen, M. Kuittinen, H.P. Herzig, J. Eur. Opt. Soc.-Rapid 13 (2017) 5.

Qianru Yang received her Bachelor degree in Optical Information Science and Technology from Harbin University of Science and Technology in 2015. She is now a Master student in the School of Optoelectronic Information Science and Engineering, College of Physics, Optoelectronics and Energy, Soochow University, China. Her current research interests focuses on the light-trapping design of graphene and the optical sensing.

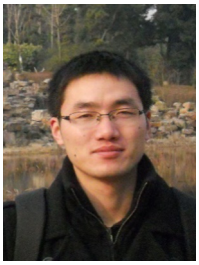

Cheng Zhang received his B.Eng. degree from Soochow University in 2013. He is now a Ph.D. candidate in the School of Optoelectronic Information Science and Engineering, College of Physics, Optoelectronics and Energy, Soochow University, China. His research interests include the high-performance hot-carrier photodetection application and advanced light-trapping designs for solar cells and photoconversion devices. He has published over 20 papers in peer-reviewed journals, including first-authored 8 papers in ACS Nano, Nano Energy (2 papers), Nanoscale, Appl. Phys. Lett., et al. He is the recipients of 4 scholarships, such as the National Scholarship for Postgraduate Students of China, the Excellent Postgraduate Students of Soochow University, etc.

Prof. Shaolong Wu received the B.S. degree in Applied Physics from Nanchang University, China, in 2008, and the Ph.D. degree in Condensed Matter Physics from Beijing Normal University, China, in 2013. He is currently working as an associate professor in the School of Optoelectronic Information Science and Engineering, College of Physics, Optoelectronics and Energy, Soochow University, China. He has authored and co-authored more than 40 scientific articles. His current research interests focus on micro/nanostructure fabrication, solar energy conversion, and photon detection.

Dr. Shaojuan Li is a lecturer at Institute of Functional Nano and Soft Materials (FUNSOM), Soochow University, China. She received her B.E. Degree (2007) from Shandong University (China) in Information Science and Engineering. She received her Ph.D. degree (2013) from Peking University (China) in Microelectronics and Solid Electronics prior to joining in FUNSOM in 2013. Her research interests include transistors and optoelectronic devices based on two-dimensional materials.

Prof. Qiaoliang Bao received his B.A. (2000) and M.E. (2003) degrees in Materials Science and Engineering from Wuhan University of Technology (China). He obtained his Ph.D. degree (2007) in Materials Physics and Chemistry from Wuhan University (China). He worked as postdoctoral fellow at Nanyang Technological University and National University of Singapore from 2007 to 2012. He has authored or co-authored more than 110 refereed journal articles with more than 10,000 total citations. His research interests include synthesis and optical characterization of two-dimensional materials as well as their incorporation into photonic and optoelectronic devices.

Dr. Vincenzo Giannini started his scientific adventure as Physics undergraduate students at the University of Pisa. Later, he moved to Spain for a Ph.D. program at the Spanish research council (CSIC) in Madrid. He worked as a postdoc in Amsterdam and a Marie Curie fellowship at the Imperial College London after Madrid. In June 2014, he started his group at the Imperial College London in the Condensed Matter Theory section. He recently accepted an offer in Spain at the CSIC. His scientific interests rely on theoretical light-matter interactions, in particular, theoretical linear and nonlinear Plasmonics and Nanophotonics.

Prof. Stefan A. Maier holds the Chair in Hybrid Nanosystems at Ludwig-Maximilians-Universität München, and the Lee-Lucas Chair in Physics at Imperial College London. He is a fellow of the Optical Society of America and of the Institute of Physics.

Prof. Xiaofeng Li received B.Eng. (2002) and Ph.D. (2007) degrees from Southwest Jiaotong University, China, and has been working in Nanyang Technological University and Imperial College London for 5 years. Since 2012, he is working at Soochow University as a distinguished professor and was selected by "Thousand Young Talents Program" of China. His interests include photovoltaics, surface-plasmons, and advanced photoconversions, with > 100 journal publications and > 30 invited talks. He is senior member of IEEE and Optical Society of China, member of OSA and SPIE, Topical Editor of OSA Applied Optics, associate editor of IEEE Photonics Journal, and Editorial Board Member of Scientific Reports.